



Impedance estimation for robot contact with uncalibrated environments



Wenrui Wang^{a,b}, Qinwen Li^{a,b}, Chenghua Lu^{a,b}, Jinlin Gu^{a,b}, Ang Li^a, Yanhui Li^a, Qi Huo^a, Hairong Chu^a, Mingchao Zhu^{a,*}

^a Changchun Institute of Optics, Fine Mechanics and Physics, Chinese Academy of Sciences, Changchun 130033, China

^b University of Chinese Academy of Sciences, Beijing 100049, China

ARTICLE INFO

Article history:

Received 6 October 2020

Received in revised form 12 February 2021

Accepted 26 February 2021

Available online 19 March 2021

Keywords:

Unknown impedance parameters

Uncalibrated environment position

Online estimation

Position and force switching controller

BFGS method

ABSTRACT

This paper examines the problem of online estimation of the environment impedance parameters and position during the contact of a robot with an uncalibrated environment. Position controllers are commonly used for free motion, while force controllers are used for constrained motion of robots. However, it is not trivial to set controller parameters for practical contact tasks with unknown environments. In particular, the environmental position is uncalibrated, and it is impossible to determine the contact position through force sensor information because of the presence of a force measurement threshold. To this end, an estimation algorithm based on L-BFGS is proposed to obtain the environmental impedance parameters and position. The estimated environment position is updated with the impedance parameters, and the impedance parameter estimation is directly related to the penetration position. The penetration position is determined by the real position of manipulators and environment surface position. The estimated environmental parameters are used to modify the position and force switching controller parameters; therefore, the accuracy of these parameters can be evaluated by the performance of the modified controller. Simulations and experiments are successfully conducted and validated with the proposed impedance estimation method. The accuracy and effectiveness of the algorithm is verified through the force and trajectory tracking performance in simulations and experiments.

© 2021 Elsevier Ltd. All rights reserved.

1. Introduction

Since robots are being more widely deployed in all aspects of production and life, they are not only just required to perform simple repetitive tasks in static environments. Studying the interaction between robots and different environments has become an important topic in robot controller design. Position and force switching controllers are always applied to interactive tasks to guarantee the performance of trajectory and force tracking regardless of the free motion or contact phase. Here, a virtual semi-active damping controller [1] is employed in this paper, and the controller is improved to suppress the bouncing [2] in the transition phase without reducing the contact speed. As one of the most commonly used interactive

* Corresponding author.

E-mail addresses: wangwenrui93@outlook.com (W. Wang), liqinwen93@163.com (Q. Li), luchenghua18@mails.ucas.ac.cn (C. Lu), jinlingu940822@163.com (J. Gu), bcleon@126.com (A. Li), liyanhui-1986@163.com (Y. Li), 514590249@qq.com (Q. Huo), chuhr@ciomp.ac.cn (H. Chu), zhumingchao@ciomp.ac.cn (M. Zhu).

control methods, impedance control is directly affected by the mechanical characteristics of the contact environment [3,4]. The controller parameters are updated with the environmental parameters, so it is critical to accurately obtain the parameters of contact dynamics models [5] in different environments.

An accurate description of the contact dynamics can make the robot controller better adapt to the current working conditions. A scheme based on artificial neural network is developed to provide a new and feasible approach for the research of contact/impact process between complex contacting surfaces by utilizing the data-driven modelling framework [6]. The genetic algorithm sequential quadratic programming (GA-SQP) hybrid estimation method is employed to obtain the unknown contact dynamical parameters under each initial indentation velocity [7]. Iterative learning impedance methods are adopted to obtain the desired impedance model with better performance [8,9]. Impedance parameters are modulated by learning neural networks, although this requires expensive data preprocessing to train the samples [10,11]. Reinforcement learning methods such as the PI2 (policy improvement with path integrals) algorithm [12] and iterative linear-quadratic-gaussian (iLQG) [13], enable the execution of various contact tasks indifferent environments by applying impedance control to the robots. Most of the mentioned methods use the position and velocity of the robot end-effector and the forces that act on the end-effector to estimate the impedance parameters; furthermore, the penetration depth of the probe is always considered known [14]. However, the environmental surface position is difficult to accurately obtain without visual information assistance or calibration in advance [15], when a robot interacts with different environments in the actual application process.

Several studies on impedance estimation taking into account the environment position. A Kalman filter-based algorithm is presented to estimate both the environmental contact dynamics parameters and geometric parameters such as the environment position and orientation [16]. Unfortunately, the state space model contains a discontinuity because of the employed switching controller, which causes a significant amount of bimodality [17], such that the estimation method based on the Kalman filter cannot be successfully applied in this situation. A least-square-based method is developed to identify the contact parameters from complex stiff multi-point contact scenarios [18]. Moreover, a hybrid contact modelling (HCM) method is presented to accurately simulate practical contact scenarios by combining a physics-based contact model and a data-driven error model [19]. Although these two methods can overcome the effect of a discontinuity, the noise of the measured force information is not fully considered. In particular, they do not consider the effects of the nonzero state of the measured force in the free motion and the force overshoot in the contact transition process on the environmental parameter estimation. Considering the switching controller focused in this paper, the measured force is a critical judgement about mode switching [20]. Basically, whether the measured value of the force sensor is zero is commonly used as a basic judgement for whether the robot is in contact with the environment [21]. Because the measured force is noisy, it is impossible for the force to always be zero in the noncontact state. To this end, a measurement threshold is generally set for the force sensor. When the measured force is not greater than it, the force exerted on the robot probe is considered zero. However, if there is a force measurement threshold, it is a substantial challenge for both environment parameter estimation and controller design.

In this paper, the estimated parameters are used to modify the controller parameters of the position and force hybrid controller based on virtual semi-active damping. If the measured force information is still used as a judgement for the controller mode conversion, the position of the control mode conversion is not on the environmental surface because of the existence of this threshold. To address environmental position uncertainties, not only the environmental dynamics parameters but also the environmental position should be identified. Therefore, an impedance estimation method based on L-BFGS for robot contact with uncalibrated environment is proposed. The L-BFGS (limited-memory BFGS) method is a nonsmooth analysis method for unconstrained optimization, and it is not affected by a discontinuity. Moreover, unlike these learning methods, the proposed L-BFGS impedance estimation method is based on a clear environmental dynamics model and has a simpler framework, which enables practical implementation. The online estimation method is developed under a switched system controller framework to identify the environmental constraints. Therefore, the performance of the controller can be used to evaluate the accuracy of the estimated parameters. This paper aims to combine the online estimation and the evaluation of the estimation results, which is of great significance in practical applications.

The remainder of this paper is organized as follows. In Section 2, a model of the contact between the manipulator and the environment is established, meanwhile, and a switching motion-force controller based on virtual semi-active damping is also designed. Section 3 discusses the details of the proposed impedance estimation algorithm based on L-BFGS. In Section 4 and Section 5, simulations and experiments are conducted by letting manipulators contact with different environments to verify the correctness and feasibility of the proposed method. Thereafter, the conclusions are drawn in Section 6.

2. System modeling and controller design

In most cases, when the manipulator interacts with the environment, only one DOF of the end-effector of the manipulator is affected. Considering the simplified interaction model in Fig. 1, the dynamics equation is expressed as:

$$M\ddot{\mathbf{p}} + \mathbf{b}\dot{\mathbf{p}} + \mathbf{F}_e = \mathbf{F}_c, \quad (1)$$

where $\mathbf{p} \in \mathbb{R}^3$ is the manipulator position, M is an equivalent mass for control and $\mathbf{b} \in \mathbb{R}^{3 \times 3}$ is the equivalent viscous friction that acts on the end effector (viscous friction \mathbf{b} is generally set $\mathbf{0}$ to prevent viscous friction from the dissipating energy [22]). $\mathbf{F}_c \in \mathbb{R}^3$ is the control force, and $\mathbf{F}_e \in \mathbb{R}^3$ is the force exchanged between the environment and the end effector.

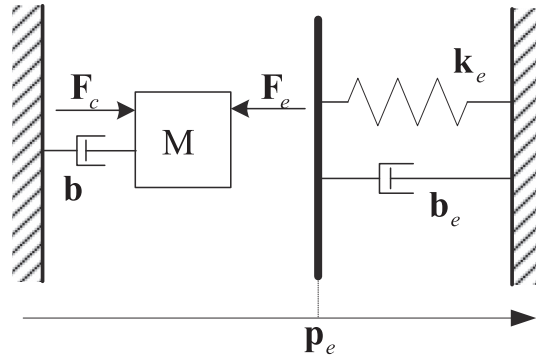


Fig. 1. 1-DOF contact model in 3D space.

The position of the environment is $\mathbf{p} = \mathbf{p}_e$, when the equivalent spring is at rest. Therefore, once the manipulator makes contact with the environment, the penetration depth of the manipulator is $\Delta\mathbf{p} = \mathbf{p} - \mathbf{p}_e$. Kelvin-Voigt linear contact model is employed to characterize the relationship between penetration and reaction force [10]

$$\mathbf{F}_e = \mathbf{k}_e \Delta\mathbf{p} + \mathbf{b}_e \Delta\dot{\mathbf{p}}, \tag{2}$$

where \mathbf{k}_e and \mathbf{b}_e are the matrices of the stiffness and damping of the environment, respectively. These matrices depend on the dynamic properties of the end-effector and environment and their contact configuration. They are both symmetric matrices in a generally accepted sense of the term [23]. Without considering the effect of the shape of the end-effector, there is a rotation matrix \mathbf{R}_e , such that

$$\mathbf{k}_e = \mathbf{R}_e \begin{bmatrix} k_x & & \\ & k_y & \\ & & k_z \end{bmatrix} \mathbf{R}_e^T, \mathbf{b}_e = \mathbf{R}_e \begin{bmatrix} b_x & & \\ & b_y & \\ & & b_z \end{bmatrix} \mathbf{R}_e^T \tag{3}$$

where k_x, k_y, k_z, b_x, b_y and b_z are the principal translational stiffness and damping in the directions that correspond to the columns of the rotation matrix [24], respectively. Moreover, \mathbf{R}_e can be considered an identity matrix that neglects the coupling of stiffness and damping and the friction force. Because \mathbf{k}_e and \mathbf{b}_e are diagonal, the force of the environment acting on the manipulator in each direction can be written as $F_e = k_e \Delta p + b_e \Delta \dot{p}$ (k_e and b_e are the stiffness and damping coefficient corresponding to the force F_e direction; Δp and $\Delta \dot{p}$ are the penetration depth and velocity).

The present work aims to control the manipulator so that it follows a desired trajectory $\mathbf{p}_d(t)$ in free motion and regulate a desired force profile $\mathbf{F}_d(t)$ in the contact phase. The simplest strategy that accomplishes the described task is to switch between a position controller and a force controller. In each direction, the switch of the controller is realized by detecting whether the manipulator is in contact with the environment; i.e., the controller is a position controller when $\Delta p \leq 0$ and a force controller otherwise. However, the surface of the environment is unknown without calibration. The switching between position and force control modes cannot rely on whether $\Delta p > 0$. The most widely used method to determine whether a robot is in contact with the environment is whether the contact force $F = 0$ [21].

The two controllers are commonly a resolved acceleration controller and a proportional force controller [22]. However, this closed-loop switching system cannot prevent the bounce of the manipulator from contacting a rigid environment unless a high-damping controller is used during contact. To this end, a position force hybrid controller is designed based on virtual semiactive damping [1], and the controllers are switched by detecting the measured force F ,

$$\mathbf{F}_c = \begin{cases} M\ddot{\mathbf{p}}_d + \mathbf{k}_{p1}(\mathbf{p} - \mathbf{p}_d) + \mathbf{k}_d\dot{\mathbf{p}} & \|\mathbf{F}\| = 0 \\ \mathbf{F}_d + \mathbf{k}_{p2}\Delta\mathbf{F} - \mathbf{b}_{sem}\dot{\mathbf{p}} & \|\mathbf{F}\| > 0 \end{cases} \tag{4}$$

where $\mathbf{k}_{p1} = \text{diag}(k_{p1}^x, k_{p1}^y, k_{p1}^z)$ and $\mathbf{k}_{p2} = \text{diag}(k_{p2}^x, k_{p2}^y, k_{p2}^z)$ are the proportional gains of the motion and force controller. $\mathbf{k}_d = \text{diag}(k_d^x, k_d^y, k_d^z)$ is the derivative gain of the motion controller, $\Delta\mathbf{p}$ and $\Delta\mathbf{F}$ are the position and force error, respectively, and $\mathbf{b}_{sem} = \text{diag}(b_{sem}^x, b_{sem}^y, b_{sem}^z)$ is the virtual semiactive damping. Contact force \mathbf{F} , position \mathbf{p} and velocity $\dot{\mathbf{p}}$ can be measured by sensors. There must be three directions of interaction when the manipulator contacts the environment, and the force exchanged between the environment and the manipulator also exists in three directions, so the forces in all directions must be considered in the control mode switching. Then, $\|\mathbf{F}\|$ is selected as the criterion for control mode switching. Although the measured force can be considered equal to the environmental force in the contact phase, the measured force F in one direction cannot remain at 0 in the entire free motion phase. Therefore, a threshold of $\|\mathbf{F}\|$ is introduced, and it is set as β . When the measured value of the force sensor is not greater than β , it is assumed that the robot is not in contact with the environment, and the force that acts on the robot in all directions is zero.

The virtual semiactive damping \mathbf{b}_{sem} works in the force control phase and is defined as

$$\mathbf{b}_{sem} = \mathbf{b}_f + \mathbf{b}_v, \tag{5}$$

where $\mathbf{b}_f = \text{diag}(b_f^x, b_f^y, b_f^z)$ is the damping gain, dissipating energy during the contact phase, and $\mathbf{b}_v = \text{diag}(b_v^x, b_v^y, b_v^z)$ is the virtual damping that can be actively modulated. A semiactive damper based on the position error is considered [25], as shown in Fig. 2. The damping prevents the manipulator from moving away from the desired position, which implies that a stronger damping force acts further from the desired position. Therefore, b_v is considered virtual active damping in any of the three directions, and b_v is defined as

$$b_v = \begin{cases} \min [\lambda|p - p_{fd}|, b_{v,max}] & \|\mathbf{F}\| \geq \beta \\ 0 & \|\mathbf{F}\| < \beta \end{cases} \tag{6}$$

Here, the virtual semi-active damping in the three directions is uncoupled, so Eq. (6) only focuses on one direction. $\lambda > 0$ is the gain coefficient of damping and position error, while $b_{v,max}$ is the saturation point for the damping coefficient. Additionally, p_{fd} is the virtual desired position that corresponds to the desired contact force F_d in the same direction, which satisfies $k_e(p_{fd} - p_e) + b_e\dot{p}_{fd} = F_d$. It is assumed that the manipulator tracks only a constant force in each direction. The velocity of the manipulator is $\dot{p}_{fd} = 0$ in the steady state for a constant desired force; otherwise, the system oscillates. Therefore, the damping effect can be ignored in this case, p_{fd} only must satisfy $k_e(p_{fd} - p_e) = F_d$. Therefore, it is considered that there is a desired p_{fd} , which corresponds to the desired contact force F_d in the contact phase, where $p_{fd} = F_d/k_e + p_e$.

For this switching controller, the semiactive damping comprises b_f and b_v , where b_f is the fixed damping gain, while $b_v = \lambda|p - p_{fd}|$ is the active damping gain simulated by position feedback. Without considering that the contact phase p is much larger than p_{fd} , the damping is maximum when $p = 0$, i.e., when the robot has only touched the environment. Large damping can suppress the force overshoot. The value of λ can be changed in an allowable range according to the actual needs to adjust the peak value and rate of change of damping to better suppress the overshoot. When the manipulator approaches p_{fd} , the damping will decrease, which is beneficial for saving energy. In this regard, an accurate estimation of the environmental dynamic parameters and surface position can ensure that the controller has good performance.

3. Identification of Environment Parameters

As mentioned in Section 2, the stiffness and damping in each direction are uncoupled, so an impedance estimation strategy is designed to estimate the impedance parameters in a single direction; it can be applied to all three translational directions in Cartesian space. However, the control model switching depends on $\|\mathbf{F}\|$, i.e., Whether contact occurs, it is determined by the force that acts on the manipulator in three directions. Meanwhile, the impedance identification algorithm begins when the contact occurs.

3.1. Identification algorithm based on the L-BFGS method

The environmental impedance only works when the manipulator makes contact with the environment. The main control target during contact is the contact force. Therefore, to develop an impedance estimation algorithm, a cost function is defined to measure the contact performance

$$J = (F - \tilde{k}\Delta p - \tilde{b}\Delta\dot{p})^2, \tag{7}$$

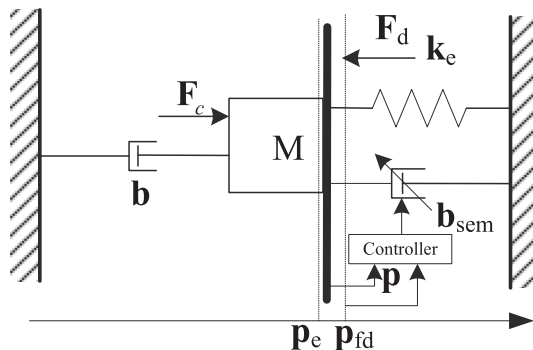


Fig. 2. Contact model with virtual semi-active damping.

where \tilde{k} and \tilde{b} are the estimated values of environmental stiffness and impedance, respectively; $\Delta p = p - p_e$ and $\Delta \dot{p} = \dot{p}$ are the penetration depth and velocity of the manipulator, respectively, in one direction. F, p and \dot{p} are the force, position, and velocity measured by the sensors. The cost function can be modified as

$$J = (F - \tilde{k}(p - \tilde{p}_e) - \tilde{b}\dot{p})^2. \tag{8}$$

Since p_e is obtained according to the actual position of the manipulator and estimated stiffness, it is expressed as

$$\tilde{p}_e = p - \Delta p = p - \frac{F - \tilde{b}\dot{p}}{\tilde{k}}. \tag{9}$$

Therefore, $\min J(\tilde{k}, \tilde{b})$ must be solved to achieve better contact performance. Unconstrained optimization variable metric algorithms are adopted for such iterative problems. The position and velocity of the manipulator are bounded, so it is assumed that J is strongly convex in the iteration interval. Letting $\mathbf{z} = [\tilde{k} \ \tilde{b}]$ and adopting the Taylor expansion of the function at \mathbf{z}^{k+1} and ignoring quadratic and higher terms, $J(\mathbf{z})$ is written as

$$J(\mathbf{z}) = J(\mathbf{z}^{k+1}) + \nabla J(\mathbf{z}^{k+1})^T (\mathbf{z} - \mathbf{z}^{k+1}) + \frac{1}{2} (\mathbf{z} - \mathbf{z}^{k+1})^T \nabla^2 J(\mathbf{z}^{k+1}) (\mathbf{z} - \mathbf{z}^{k+1}), \tag{10}$$

where

$$\nabla J(\mathbf{z}^{k+1}) = \begin{bmatrix} \frac{\partial J}{\partial k} \\ \frac{\partial J}{\partial b} \end{bmatrix} = \begin{bmatrix} -2\Delta p^{k+1} (F - \tilde{k}\Delta p^{k+1} - \tilde{b}\dot{p}^{k+1}) \\ -2\dot{p}^{k+1} (F - \tilde{k}\Delta p^{k+1} - \tilde{b}\dot{p}^{k+1}) \end{bmatrix} \tag{11}$$

and

$$\nabla^2 J(\mathbf{z}^{k+1}) = \begin{bmatrix} \frac{\partial^2 J}{\partial k^2} & \frac{\partial^2 J}{\partial k \partial b} \\ \frac{\partial^2 J}{\partial k \partial b} & \frac{\partial^2 J}{\partial b^2} \end{bmatrix} = \begin{bmatrix} -2(\Delta p^{k+1})^2 & -2\Delta p^{k+1}\dot{p}^{k+1} \\ -2\Delta p^{k+1}\dot{p}^{k+1} & -2(\dot{p}^{k+1})^2 \end{bmatrix}. \tag{12}$$

Letting $\mathbf{z} = \mathbf{z}^{k+1}$, $\Delta p^{k+1} = p^{k+1} - p_e^k$, the gradient for Eq. (10) is obtained

$$\nabla J(\mathbf{z}^{k+1}) - \nabla J(\mathbf{z}^k) = \nabla^2 J(\mathbf{z}^{k+1} - \mathbf{z}^k), \tag{13}$$

when $\nabla J(\mathbf{z}^k) = 0$,

$$\mathbf{z}^{k+1} = \mathbf{z}^k + (\nabla^2 J(\mathbf{z}^{k+1}))^{-1} \nabla J(\mathbf{z}^{k+1}), \tag{14}$$

where $\nabla^2 J(\mathbf{z}^{k+1})$ is the Hessian matrix \mathbf{H} . \mathbf{H} is iteratively updated based on the data measured by sensors. However, the speed must be equal to zero during the motion, so \mathbf{H} is irreversible and prevents us from adopting Newton method. The BFGS algorithm is introduced, and it is a typical implementation of the quasi-Newton method.

Eq. (11) is abbreviated as

$$\mathbf{y}^k = \mathbf{H}^{k+1} \mathbf{s}^k, \tag{15}$$

where $\mathbf{y}^k = \nabla J(\mathbf{z}^{k+1}) - \nabla J(\mathbf{z}^k)$, $\mathbf{s}^k = \mathbf{z}^{k+1} - \mathbf{z}^k$. In this case, \mathbf{s}^k can also be expressed as $\mathbf{s}^k = (\mathbf{H}^{k+1})^{-1} \mathbf{y}^k$. An approximation matrix can be constructed for the matrix \mathbf{H}

$$\mathbf{B}^k \approx \mathbf{H}^k, \tag{16}$$

where \mathbf{B}^k is updated according to

$$\mathbf{B}^{k+1} = \mathbf{B}^k + \Delta \mathbf{B}^k. \tag{17}$$

The initial value of the matrix \mathbf{B}^0 is the identity matrix \mathbf{I} . The problem that must be solved is to modify the construction of the matrix $\Delta \mathbf{B}^k$ in each iteration. The calculation formula is

$$\Delta \mathbf{B}^k = \frac{\mathbf{y}^k (\mathbf{y}^k)^T}{(\mathbf{y}^k)^T \mathbf{s}^k} - \frac{\mathbf{B}^k \mathbf{s}^k (\mathbf{s}^k)^T \mathbf{B}^k}{(\mathbf{s}^k)^T \mathbf{B}^k \mathbf{s}^k}. \tag{18}$$

The next iterate \mathbf{z}^{k+1} is

$$\mathbf{z}^{k+1} = \mathbf{z}^k + \gamma^k \mathbf{d}^k, \tag{19}$$

where $\mathbf{d}^k = -(\mathbf{B}^k)^{-1} \nabla J(\mathbf{z}^k)$ is the search direction, and $\gamma^k > 0$ is the step length. Applying Sherman-Morrison equation, the relationship between $(\mathbf{B}^{k+1})^{-1}$ and $(\mathbf{B}^k)^{-1}$ is obtained

$$\begin{aligned} (\mathbf{B}^{k+1})^{-1} &= \left(\mathbf{I} - \frac{\mathbf{s}^k (\mathbf{y}^k)^T}{(\mathbf{y}^k)^T \mathbf{s}^k} \right) (\mathbf{B}^k)^{-1} \left(\mathbf{I} - \frac{\mathbf{y}^k (\mathbf{s}^k)^T}{(\mathbf{y}^k)^T \mathbf{s}^k} \right) + \frac{\mathbf{s}^k (\mathbf{s}^k)^T}{(\mathbf{y}^k)^T \mathbf{s}^k} \\ &= (\mathbf{B}^k)^{-1} + \left(\frac{1}{(\mathbf{s}^k)^T \mathbf{y}^k} + \frac{(\mathbf{y}^k)^T (\mathbf{B}^k)^{-1} \mathbf{y}^k}{((\mathbf{s}^k)^T \mathbf{y}^k)^2} \right) \mathbf{s}^k (\mathbf{s}^k)^T \\ &\quad - \frac{1}{(\mathbf{s}^k)^T \mathbf{y}^k} \left((\mathbf{B}^k)^{-1} \mathbf{y}^k (\mathbf{s}^k)^T + \mathbf{s}^k (\mathbf{y}^k)^T (\mathbf{B}^k)^{-1} \right) \end{aligned} \tag{20}$$

In the implementations of the BFGS algorithm, $\gamma^k > 0$ satisfies Wolfe conditions [26]:

$$J(\mathbf{z}^k + \gamma^k \mathbf{d}^k) \leq f(\mathbf{z}^k) + \delta_1 \gamma^k (\mathbf{d}^k)^T \nabla J(\mathbf{z}^k), \tag{21}$$

$$(\mathbf{d}^k)^T \nabla J(\mathbf{z}^k + \gamma^k \mathbf{d}^k) \geq \delta_2 (\mathbf{d}^k)^T \nabla J(\mathbf{z}^k), \tag{22}$$

where δ_1 and δ_2 are constants such that $0 < \delta_1 \leq \delta_2 < 1$. When the objective function $J(\mathbf{z})$ is convex, if Wolfe conditions of an inexact linear search are satisfied, this algorithm is globally convergent. The pseudocode of the impedance estimation algorithm is presented in Algorithm 1.

Algorithm 1: Environment impedance parameters and position estimation algorithm based on L-BFGS method

Input:

Initial iterate $\mathbf{z}^0 \in R^2$, initial step-length γ_0 , constants δ_1 and δ_2 and sufficiently small value ε

Output: \mathbf{z}^k

- 1: **if** $F \geq \beta$ **then**
 - 2: **while** $\nabla J(\mathbf{z}) > \varepsilon$ **do**
 - 3: Compute $\mathbf{d}^k = -(\mathbf{B}^k)^{-1} \nabla J(\mathbf{z}^k)$
 - 4: Find γ^k satisfying Wolfe line search conditions Eq. (21) and Eq. (22)
 - 5: Compute $\mathbf{z}^{k+1} = \mathbf{z}^k + \gamma^k \mathbf{d}^k$
 - 6: Compute $p_e^{k+1} = p^k - (F - \mathbf{z}^{k+1}(2)\dot{p}^k) / \mathbf{z}^{k+1}(1)$
 - 7: Compute $\dot{p}^{k+1} = p^{k+1} - p_e^{k+1}$
 - 8: Compute $(\mathbf{B}^{k+1})^{-1}$ according to Eq. (20)
 - 9: $k = k + 1$
 - 10: **end while**
 - 11: **end if**
-

3.2. Convergence analysis

To prove the global convergence of the L-BFGS algorithm, the following proposition is considered. This proposition is an important tool to analyse the L-BFGS method.

Proposition 1. The selected cost function $J(\mathbf{z})$ satisfies the following.

- (a) The objective function $J(\mathbf{z})$ is twice continuously differentiable [27].
- (b) The level set $\Omega = \{ \mathbf{z} \in R^2 : J(\mathbf{z}) \leq J(\mathbf{z}_0) \}$ is convex.
- (c) There exist positive constants M_1 and M_2 such that [28]

$$M_1 \mathbf{I} \leq \nabla^2 J(\mathbf{z}) \leq M_2 \mathbf{I}$$

By Proposition 1(c) and $\mathbf{y}^k = \mathbf{H}^{k+1} \mathbf{s}^k$ [29],

$$\mathbf{M}_1 \|\mathbf{s}^k\|^2 \leq (\mathbf{y}^k)^T \mathbf{s}^k \leq \mathbf{M}_2 \|\mathbf{s}^k\|^2, \tag{23}$$

and

$$\mathbf{M}_1 \leq \frac{\|\mathbf{y}^k\|^2}{(\mathbf{y}^k)^T \mathbf{s}^k} = \frac{(\mathbf{s}^k)^T (\mathbf{H}^{k+1})^2 \mathbf{s}^k}{(\mathbf{s}^k)^T \mathbf{H}^k \mathbf{s}^k} \leq \mathbf{M}_2. \tag{24}$$

From Eq. (23) and Eq. (24), the trace of the Hessian approximation can be estimated as

$$\begin{aligned} \text{tr}(\mathbf{B}^{K+1}) &= \text{tr}(\mathbf{B}^K) - \frac{\|\mathbf{B}^k \mathbf{s}^k\|^2}{(\mathbf{s}^k)^T \mathbf{B}^k \mathbf{s}^k} + \frac{\mathbf{y}^k (\mathbf{y}^k)^T}{(\mathbf{y}^k)^T \mathbf{s}^k} \\ &\leq \text{tr}(\mathbf{B}^K) + \frac{\mathbf{y}^k (\mathbf{y}^k)^T}{(\mathbf{y}^k)^T \mathbf{s}^k} \\ &\leq \text{tr}(\mathbf{B}^k) + \mathbf{M}_2 \\ &\leq \text{tr}(\mathbf{B}^0) + k\mathbf{M}_2 \\ &\leq \mathbf{M}_3 \end{aligned} \tag{25}$$

\mathbf{M}_3 is a positive constant. Then to bound the determinant, it can be written as

$$\begin{aligned} \det(\mathbf{B}^{K+1}) &= \det(\mathbf{B}^K) \det\left(I - \frac{\mathbf{s}^k (\mathbf{s}^k)^T \mathbf{B}^k}{(\mathbf{s}^k)^T \mathbf{B}^k \mathbf{s}^k} + \frac{(\mathbf{B}^k)^{-1} \mathbf{y}^k (\mathbf{y}^k)^T}{(\mathbf{y}^k)^T \mathbf{s}^k}\right) \\ &= \det(\mathbf{B}^K) \frac{(\mathbf{y}^k)^T \mathbf{s}^k}{(\mathbf{s}^k)^T \mathbf{B}^k \mathbf{s}^k} \\ &= \det(\mathbf{B}^K) \frac{(\mathbf{y}^k)^T \mathbf{s}^k}{\|\mathbf{s}^k\|^2} \frac{\|\mathbf{s}^k\|^2}{(\mathbf{s}^k)^T \mathbf{B}^k \mathbf{s}^k} \\ &\geq \det(\mathbf{B}^K) \frac{\mathbf{M}_1}{\text{tr}(\mathbf{B}^K)} \\ &\geq \det(\mathbf{B}^K) \frac{\mathbf{M}_1}{\mathbf{M}_3} \end{aligned} \tag{26}$$

From Eq. (25) and Eq. (26), it can be concluded that there is a constant $\delta > 0$ such that

$$\cos \theta^k \equiv \frac{\mathbf{s}^k \mathbf{B}^k (\mathbf{s}^k)^T}{\|(\mathbf{s}^k)^T\| \| \mathbf{B}^k \mathbf{s}^k \|} \geq \delta. \tag{27}$$

Theorem 1. Let \mathbf{z}^0 and \mathbf{B}^0 be the initial iterations, such that $J(\mathbf{z})$ satisfies Proposition 1, and $\{\|\mathbf{B}^k\|\}$ is bounded. Then, Algorithm 1 generates a sequence $\{\mathbf{z}^k\}$ that converges to \mathbf{z}^* . Furthermore, there is a constant $r, 0 \leq r < 1$, such that [30]

$$J^k - J^* \leq r^k (J^0 - J^*)$$

According to the line search conditions, Eq. (21) and Eq. (22) and as implied by Proposition 1, Eq. (27) can be rewritten as [31]

$$J(\mathbf{z}^{k+1}) - J(\mathbf{z}^*) \leq (1 - \alpha \cos^2 \theta^k) (J(\mathbf{z}^k) - J(\mathbf{z}^*)) \tag{28}$$

where α is a constant $\alpha > 0$. Therefore, it is concluded that

$$\frac{1}{2} \mathbf{M}_1 \|\mathbf{z}^k - \mathbf{z}^*\|^2 \leq J^k - J^*, \tag{29}$$

which combined with Theorem 1, indicates the sequence $\{\mathbf{z}^k\}$ is also R-linearly convergent.

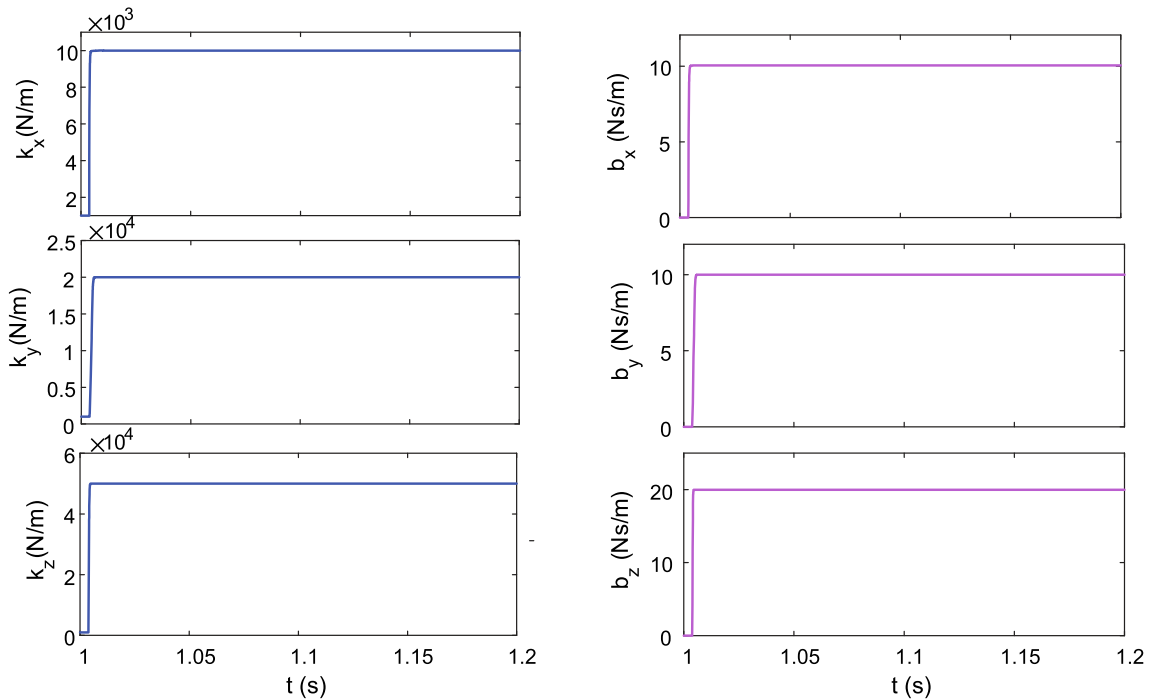
4. Simulations

In this section, a one-DOF manipulator is considered in contact with environments with different impedance parameters: a high-stiffness environment and a low-stiffness environment. The simulations are performed in the MATLAB/Simulink environment. Here, the manipulator is required to track a desired trajectory and force profile at the contact and noncontact phases, respectively. To guarantee good performance of the employed position and force switching controller, the environmental impedance parameters must be timely and accurately obtained to modify the controller parameters. Environmental parameters include impedance parameters and environmental position. The effect of the active damping modulation depends on the environment position and impedance parameters, so the performance of the controller can also be used to evaluate the accuracy of the obtained parameters. The environmental position is obtained by the measured position of the manipulator and the estimated impedance parameters according to Eq. (9), i.e., as long as the estimated impedance parameters are accurate, the exact position of the environment can be obtained.

In the first simulation, the environmental parameters are set as $\mathbf{p}_e = [x_e \ y_e \ z_e]^T = [0.05 \ 0.01 \ 0.02]^T m$, $\mathbf{k}_e = \text{diag}(k_x, k_y, k_z) = \text{diag}(10000, 20000, 50000) N/m$ and $\mathbf{b}_e = \text{diag}(b_x, b_y, b_z) = \text{diag}(10, 10, 20) Ns/m$. The desired trajectory is

$\mathbf{p}_d = [x_d \ y_d \ z_d]^T = [0.05t^2 \ 0.01t^2 \ 0.02t]^T m$ in free motion, and the desired force is $\mathbf{F}_d = [F_{dx} \ F_{dy} \ F_{dz}]^T = [102050]^T N$ in the contact phase. The controller parameters are selected as $M=1, \mathbf{k}_{p1} = \text{diag}(5000, 3000, 2000), \mathbf{k}_d = \text{diag}(100, 50, 50), \mathbf{k}_{p2} = \text{diag}(100, 50, 200), \mathbf{b}_f = \mathbf{I}$ and $\lambda = \text{diag}(20000, 10000, 50000)$. The threshold of the force sensor is $\beta = 5N$. In the impedance estimation algorithm, the same estimation parameters are set in each direction. They are $z_0 = [10000]^T, \delta_1 = 0.1, \delta_2 = 0.5$ and $\varepsilon = 10^{-3}$. By employing the impedance estimation algorithm based on the BFGS method, the environmental impedance parameters, including \mathbf{k}_e and \mathbf{b}_e , are iteratively updated, and they converge to preset values as expected (see Fig. 3). The estimation begins when $\|\mathbf{F}\| > \beta$ after $t=1s$, as shown in Fig. 3; in other words, the estimation begins after contact is made. Therefore, it is necessary to introduce the environment position estimation, and the estimation results are shown in Fig. 4. It is not difficult to find that both environmental impedance parameters and position converge to the set value. Here, the desired positions x_{fd}, y_{fd} and z_{fd} that correspond to the desired forces in three directions are not directly obtainable because of the unknown environment impedance parameters and environment position, and they must be updated with the impedance parameter and environment position (see Fig. 4). The contact environment position \mathbf{p}_e converges to $[0.050 \ 0.010 \ 0.02]^T m$ at approximately 1.005 s (see Fig. 4). The desired position p_{fd} in each direction is calculated with $p_{fd} = p_e + F_d/k_e$, where $x_{fd} = 0.05 + 10/10000 = 0.051m, y_{fd} = 0.01 + 20/20000 = 0.011m$ and $z_{fd} = 0.02 + 50/50000 = 0.021$. Through the impedance estimation algorithm, the environmental parameters, including the location, can be quickly and accurately estimated; thus, p_{fd} is quickly obtained. However, the initial stiffness estimation is set less than its real value, so there is a larger peak of p_{fd} in each direction when the estimation starts. It is beneficial to suppress the force overshoot. Moreover, the motion and force tracking results are almost identical to those controllers with the known environment (see Fig. 5) [1,32]. There is good performance in tracking both p_d (including x_d, y_d and z_d) and p_{fd} (including x_{fd}, y_{fd} and z_{fd}). Meanwhile, the force overshoot is well suppressed, and the desired forces (including f_{dx}, f_{dy} and f_{dz}) are well tracked. Therefore, the estimation algorithm enables us to obtain an accurate impedance model and guarantees the performance of virtual semidamping control.

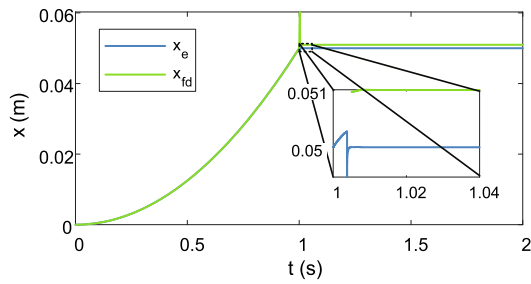
In the second simulation, the manipulator is required to contact a low-stiffness environment, the environmental parameters are set identical to those in the first simulation except the stiffness, and the stiffness matrix is $\mathbf{k}_e = \text{diag}(k_x, k_y, k_z) = \text{diag}(500, 200, 100)N/m$. Unlike the first simulation, the desired force is set as $\mathbf{F}_d = [F_{dx} \ F_{dy} \ F_{dz}]^T = [5 \ 1 \ 2]^T N$ in the contact phase, and \mathbf{k}_{p2} is selected as $\mathbf{k}_{p2} = \text{diag}(1000, 500, 2000)$. By setting the smaller desired force and selecting larger \mathbf{k}_{p2} , the convergence speed can be improved in the force control phase. Moreover, the threshold of force should be selected to be a smaller threshold, and it is set to $\beta = 1N$. In the impedance estimation algorithm, the initial value should also be a smaller value of $z_0 = [100 \ 0]^T$. The actual environmental impedance parameters are obtained by the proposed impedance estimation method, although the parameters slightly more slowly converge in this simulation. Because the initial stiffness in



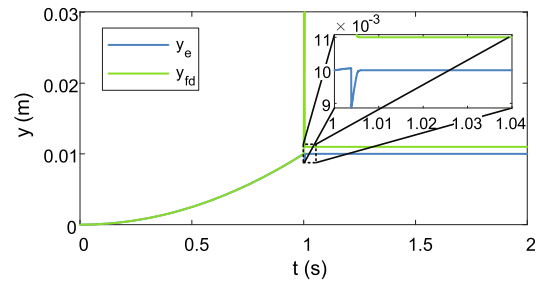
(a) Update of stiffness in three directions.

(b) Update of damping in three directions.

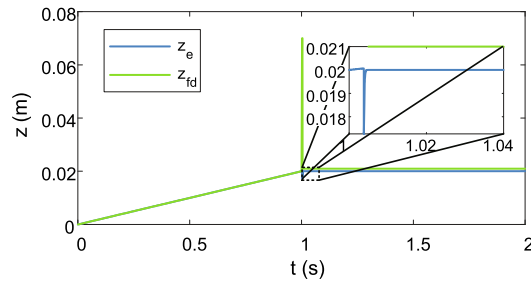
Fig. 3. Update of stiffness \mathbf{k} and damping \mathbf{b} with the impedance estimation algorithm in the first simulation.



(a) Update of environment position and virtual desired position in x direction.

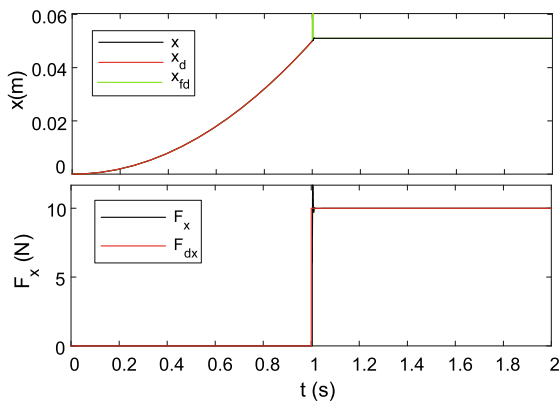


(b) Update of environment position and virtual desired position in y direction.

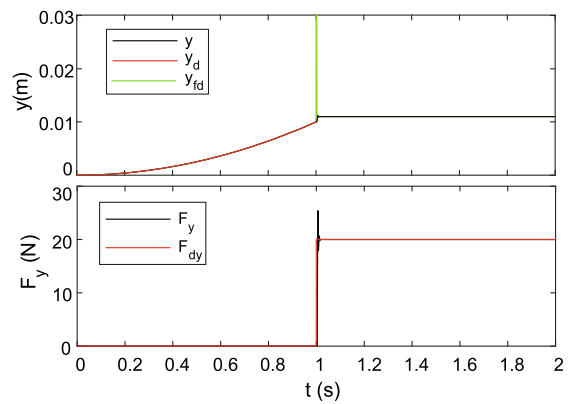


(c) Update of environment position and virtual desired position in z direction.

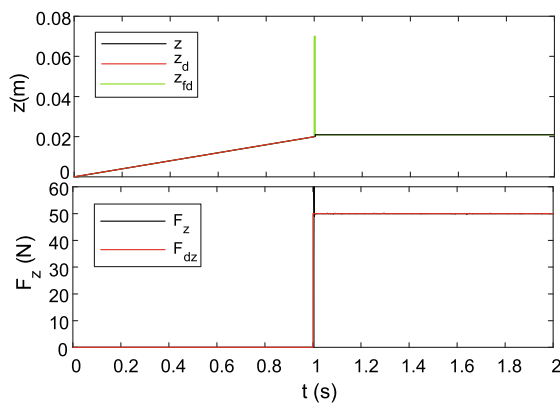
Fig. 4. Update of environment position \mathbf{p}_e and virtual desired \mathbf{p}_{fd} corresponding to the desired force in the first simulation.



(a) The position and force tracking results in x direction.



(b) The position and force tracking results in y direction.



(c) The position and force tracking results in z direction.

Fig. 5. The position and force tracking results in the first simulation.

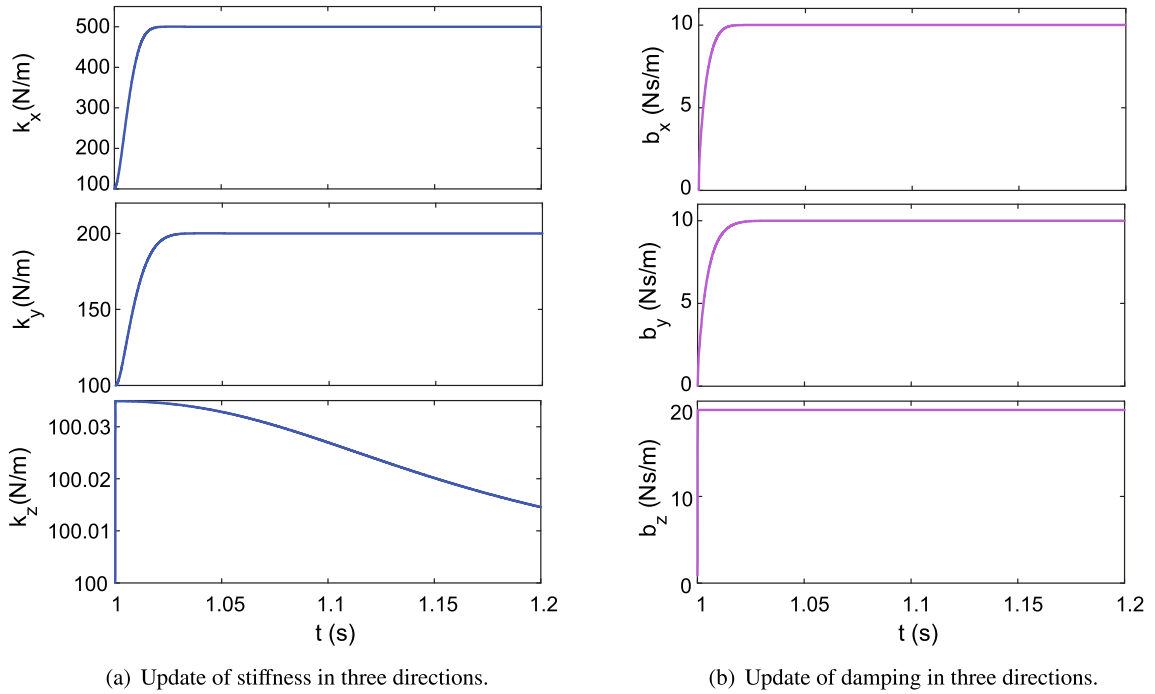
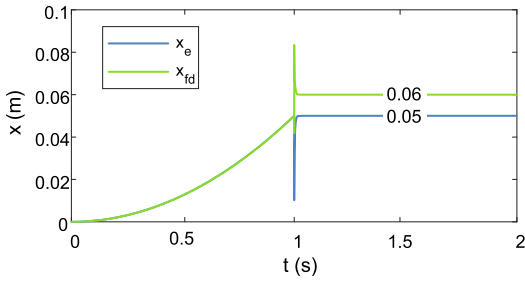


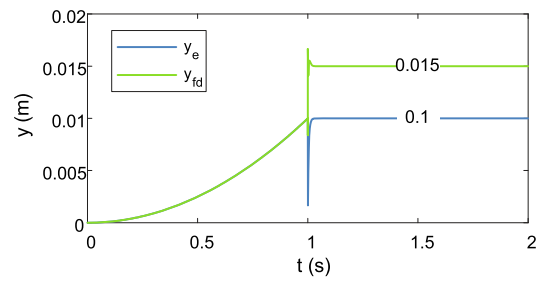
Fig. 6. Update of stiffness \mathbf{k} and damping \mathbf{b} with the impedance estimation algorithm in the second simulation.

the zdirection is identical to the real setting value, the estimation value of k_z is no more than 100.04, and b_z quickly converges to preset values. Meanwhile, the estimated environmental position in the zdirection converges faster than in other directions (see Fig. 7). Selecting an initial value close to the true value is very beneficial to the entire estimation process. The contribution of damping to the contact force is $F_x = 1N, F_y = 0.2N$ and $F_z = 0.4N$. Therefore, $\|\mathbf{F}\| = \sqrt{1 + 0.2^2 + 0.4^2} = 1.095 > \beta$ when the contact is made; furthermore, the estimation simultaneously begins (see Fig. 6). The final estimated environment positions x_e, y_e and z_e are identical to the position where the estimation starts. Nonetheless, the estimation starting position must be considered the environment position because the real damping is unknown, and it is impossible to determine whether the damping force is greater than the threshold. To this end, it is necessary to obtain the environmental parameters, including the position. x_{fd}, y_{fd} and z_{fd} are updated with the estimated environment position and stiffness, and their converged values are marked in Fig. 7. The parameters obtained by the impedance estimation algorithm based on L-BFGS are used to modify the controller parameters; then, the performance of trajectory tracking in free motion and force tracking in the contact phase is guaranteed (see Fig. 8).

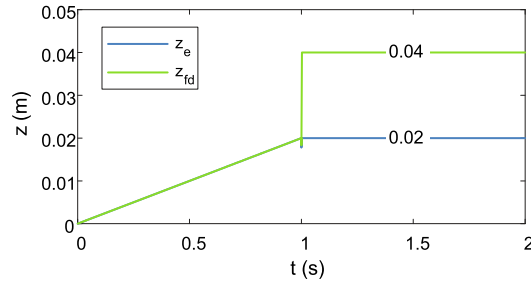
In these two simulations, let a manipulator contact different impedance environments: a high-stiffness environment and a low-stiffness environment. The damping is identical in both environments, so the contact forces are identical when contact is made with the same velocity. As mentioned, $\|\mathbf{F}\|$ is larger than β in the first simulation but less than β in the first simulation. The estimation starting time is different between Fig. 3 and Fig. 6. Moreover, when $\|\mathbf{F}_{contact}\| > \beta$ ($\mathbf{F}_{contact}$ is the force at the moment of contact) is satisfied, the position of contact force measured $\|\mathbf{F}\| > \beta$ is the actual environmental position in simulation 2, as shown in Fig. 7. However, the position where the measured value of the force sensor is greater than β cannot be considered the environment position in simulation 1, as shown in Fig. 4. In the real world, although the velocity can be measured by sensors, environmental damping is always unknown, so remains impossible to determine whether $\|\mathbf{F}_{contact}\| > \beta$. The proposed impedance estimation algorithm in this paper can ensure accurate environmental parameters, including the position, in the presence of a force measurement threshold. Using the proposed impedance method, the effect of mode switching timing can be ignored in the overall estimation process. Although the convergence rate of the impedance parameters is different in different impedance environments, the obtained environmental parameters can guarantee the good performance of the entire control system in the position and force control modes (see Fig. 5 and Fig. 8). The accurate and timely acquisition of the environment location for the uncalibrated environment is also an important basis for evaluating the impedance estimation method. If the environmental position cannot be accurately obtained, the overall control performance of the system will be greatly affected.



(a) Update of environment position and virtual desired position in x direction.

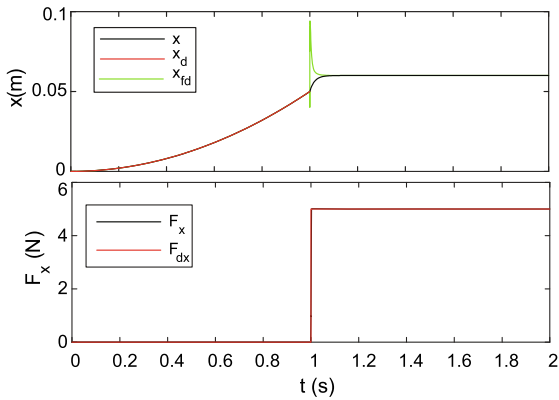


(b) Update of environment position and virtual desired position in y direction.

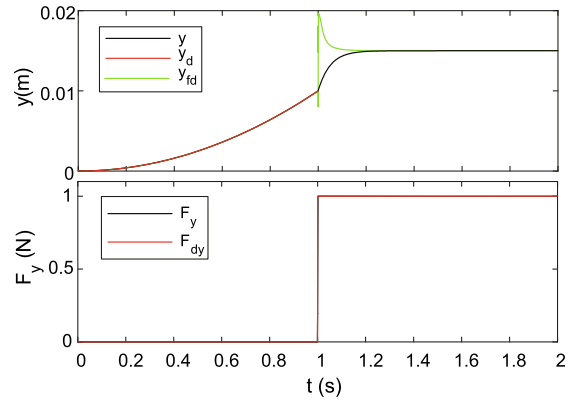


(c) Update of environment position and virtual desired position in z direction.

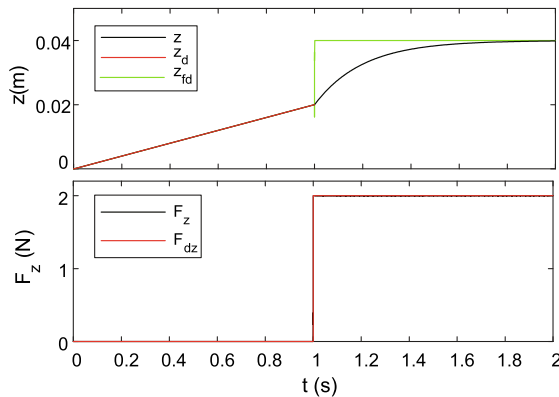
Fig. 7. Update of environment position \mathbf{p}_e and virtual desired \mathbf{p}_{fd} corresponding to the desired force in the second simulation.



(a) The position and force tracking results in x direction.



(b) The position and force tracking results in y direction.



(c) The position and force tracking results in z direction.

Fig. 8. The position and force tracking results in the second simulation.

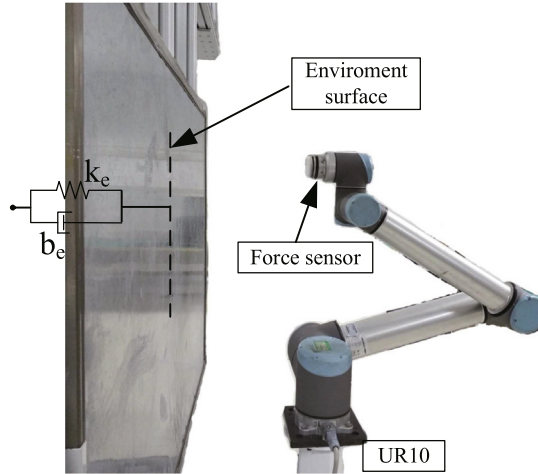


Fig. 9. Experimental set-up of contact with an aluminum plate.

5. Experiments

In this section, the impedance estimation algorithm for robot contact with an uncalibrated environment is validated using a UR10. UR10 is required to make contact with environments having different impedance parameters. A force sensor is installed at the end of the UR10 to measure the contact forces with the environment. The type of force sensor is an OptoForce HEX-70-XE-200 N with a force acquisition period of 0.01 s. The control period cannot be shorter than the force acquisition period, and experiments are performed using a 0.01-s control period. Considering the 1D case in experiments, the UR10 robot is required to move at a speed of 0.03 m/s and switch to the force control mode after contact with the environment if $\|F\| > \beta$.

In the first experiment, the UR10 robot is required to make contact with an aluminium plate (see Fig. 9), where the desired contact force is set to $F_d = 50\text{N}$, and the position of the environment is unknown. The threshold β is set as 5. By using the “speed1” instruction of UR10, the speed control mode is adopted in experiments. In this mode, the acceleration is calculated using $\ddot{p} = (F_c - F_e)/M$, and the velocity is obtained in the control period. To suppress higher acceleration in the contact phase, M is selected as a larger value than the actual mass of the force sensor; i.e., it is assumed that the robot end is equipped with a larger mass of the end-effector [33]. The controller parameter selection must satisfy the system stability requirements[1]. Thus, the controller parameters are set as $M = 10, k_{p1} = 1000, k_d = 10, k_{p2} = 10, \lambda = 500000$, and $b_f = 400$. These parameters, especially λ and b_f , are selected to make the controller perform better after the experiment has been repeated many times. For the impedance estimation algorithm, the input parameters are set as $z_0 = [1000 \ 0]^T, \delta_1 = 0.1, \delta_2 = 0.5$ and $\varepsilon = 0.1$, and the initial value of impedance estimation can be selected according to prior knowledge. After contact occurs ($\|F\| > \beta$), the controller switches to the force control model, and the environmental impedance parameters and position can be obtained through the impedance estimation algorithm based on the BFGS method, as shown in Fig. 10. With the estimation starting and the stiffness updating, the estimated p_e approaches a value below the initial value (see the last plot in Fig. 10). Although their deviation is not greater than 0.001, it affects the precision of the estimation, especially for high-stiffness environments. The environmental position should be obtained while estimating the environmental impedance. The desired trajectory consists of the preset desired trajectory p_d of the free motion phase and p_{jd} of the constrained motion phase, as shown in Fig. 11. p_{jd} updates according to the estimation of environment position p_e and stiffness k_e , and it is used in the controller. It is not difficult to find that the parameters estimated by impedance learning are used to correct the position of the environment and parameters in the controller, which ensures that the controller has a better performance in position tracking and force tracking, as shown in Fig. 11. In the contact phase, the defined virtual desired position is well tracked (see first plot in Fig. 11). The accuracy of the parameters estimated by the algorithm is verified from the tracking results.

In the second experiment, the UR10 robot is required to make contact with a balloon (see Fig. 12), where the desired contact force is set to $F_d = 10\text{N}$. Here, the threshold β is set as 0.5. In this experiment, except for b_f and λ , the selected control parameters are consistent with the first experiment. However, unlike the first experiment, smaller values of b_f and λ are selected in the force control mode. b_f and λ are set to $b_f = 50$ and $\lambda = 20000$, respectively. Without changing other parameters of the learning algorithm, the accuracy of the estimated parameters is guaranteed by setting $\varepsilon = 0.01$ and $z_0 = [50 \ 0]^T, \delta_1 = 0.1$. The estimated results of environmental impedance parameters and location are shown in Fig. 13. The position where the measured value of the force sensor is $\|F\| > \beta$ is $p = 0.23$, but the estimated environment position p_e is less than 0.22. The position with measured sensor value $\|F\| > \beta$ obviously cannot be considered the environment posi-

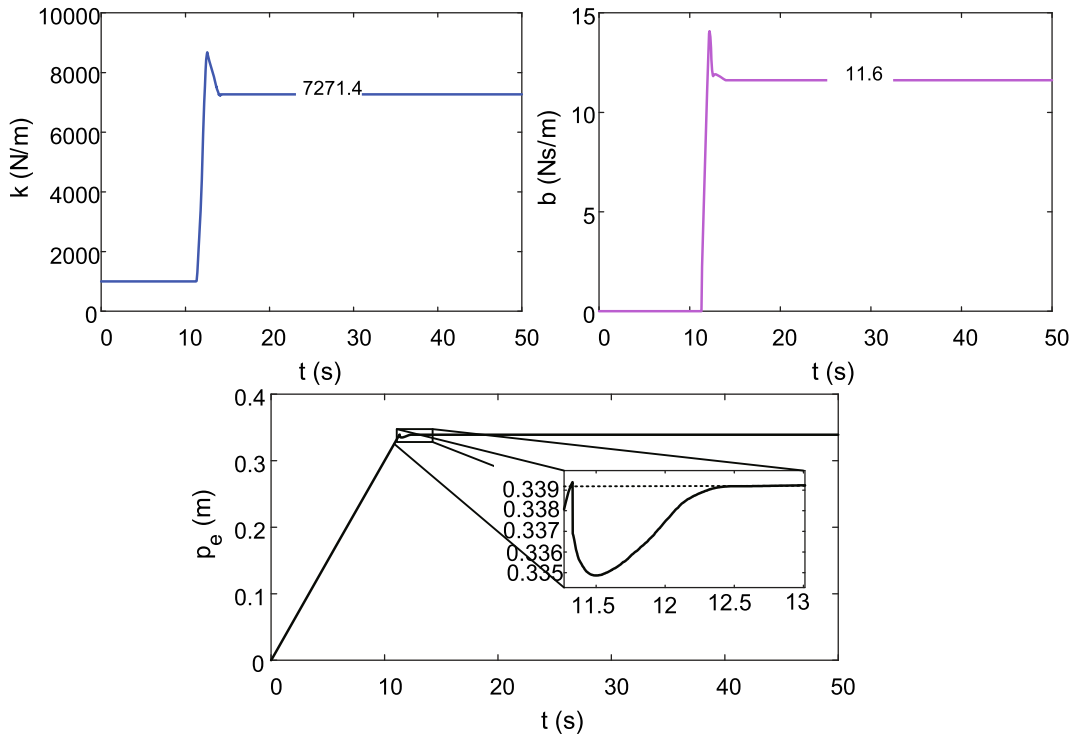


Fig. 10. Impedance parameters and environment position estimation results in the first experiment.

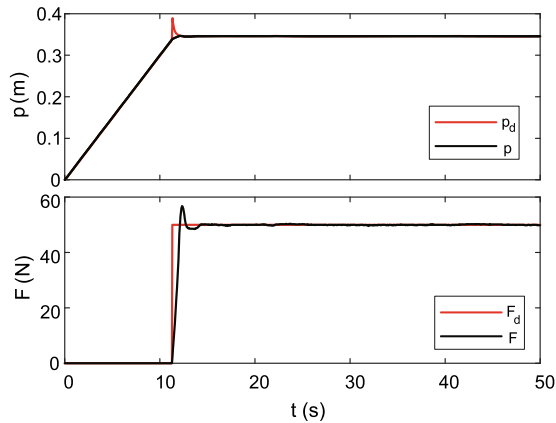


Fig. 11. Experiment results of contact with an aluminum plate.

tion, which is unfavourable to the design of the controller and contact performance of the robot. However, the contact force can be calculated with $F_{contact} = 0.03 \times 20.7 = 0.621N > \beta$, and this situation is consistent with simulation 2. However, it produces a different conclusion that the position where the estimation starts is not the environmental position. Therefore, it is not feasible to determine the environment position by a force sensor signal in the presence of a threshold. In the proposed method, the impedance parameters are used to modify the environment position. The position and force tracking results are shown in Fig. 14, and the tracking results show that the obtained impedance parameters and environment position are sufficient to ensure the performance of the controller even if they are not real.

In these two experiments, both force sensors have set threshold values β . To assure the performance of the controller, different force thresholds are set for different desired forces in the experiments. The measured value of the force sensor is considered 0 when $\|F\| < \beta$; in this case, contact is not made, and the estimation does not start. Comparing the estimated starting position with the estimated environmental position, it is found that the deviation between two positions is more obvious in the second experiment. Therefore, even $\|F\| > \beta$ can be satisfied under the effect of a damping force, as in simu-

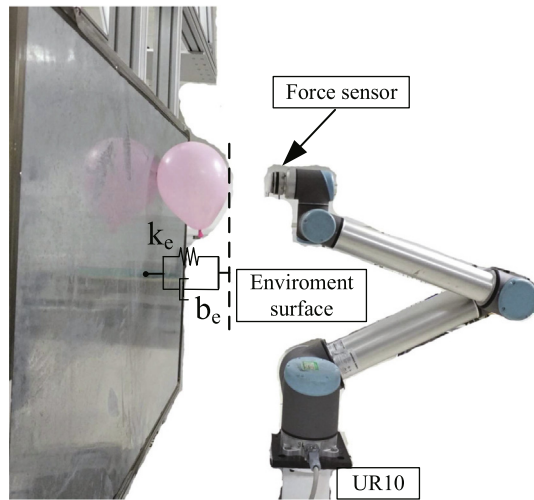


Fig. 12. Experimental set-up of contact with a balloon.

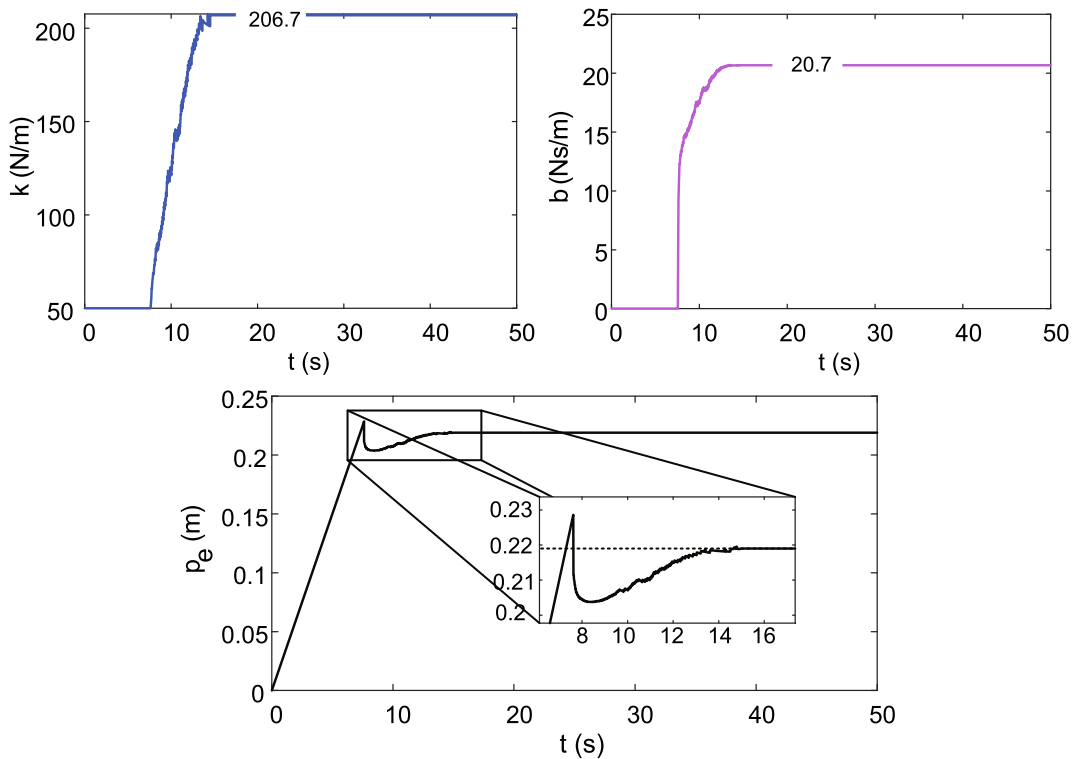


Fig. 13. Impedance parameters and environment position learning results in the second experiment.

lation 2, and it is impossible for real experiments to regard the estimation starting position as the real environment position, as shown in Fig. 13. The relation between environment position and stiffness is not linear. When the estimation algorithm is used to estimate the environmental position and stiffness, they are coupled to each other, so it is impossible to estimate the other parameter without discarding one parameter. The impedance parameters estimated by the learning algorithm and environment position are applied to the controller to modify the control parameters, and the control parameters directly determine the control effect. The accuracy of the estimated environmental parameters can be evaluated by the performance of the controller in position and force tracking. The expected force and trajectory are present in the position and force control mode with the defined $p_{fd} = p_e + F_d/sk_e$. Regardless of whether Fig. 11 or Fig. 14 is used, the virtual desired positions p_{fd} and

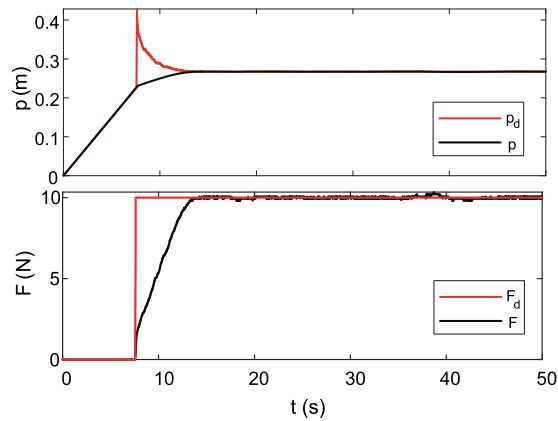


Fig. 14. Experiment results of contact with a balloon.

f_d are well tracked in the contact phase. Although the position and force of the robot slowly converge when it contacts an environment with larger damping, the overall tracking effect can still converge to the desired position and force values.

6. Conclusion

In this paper, an L-BFGS-based estimation algorithm is proposed to simultaneously estimate the impedance parameters and uncalibrated environment position online, which can address the discontinuity introduced by the switching controller and force measurement threshold. In addition, the estimated parameters can be used to modify the position and force switching controller parameters, and the performance of the controller can be adopted to evaluate the accuracy of the proposed estimation algorithm. Simulation and experimental results are presented, which illustrate the accuracy and viability of the approach. In summary, the estimation method in this study satisfies the practical application conditions, and it can be used to estimate the constraint uncertainties when manipulators are required to contact different uncalibrated environments.

This paper only focuses on the simplified impedance model, and the coupling of stiffness and damping in all directions was not considered in 3D space. As a future direction of research, the stiffness and damping matrices should not be set diagonal. The modified impedance model is closer to a real-world situation and will guarantee a better performance of the controller. Although the effects of the accuracy of the obtained environmental parameters on the controller are clarified, it is necessary to extend this approach to other control frameworks.

CRedit authorship contribution statement

Wenrui Wang: Conceptualization, Methodology, Software, Writing - original draft. **Qinwen Li:** Data curation, Writing - review & editing. **Chenghua Lu:** Data curation. **Jinlin Gu:** Resources. **Ang Li:** Software. **Yanhui Li:** Visualization, Software, Supervision. **Qi Huo:** Resources. **Hairong Chu:** Supervision. **Mingchao Zhu:** Methodology, Supervision, Writing - review & editing, Project administration.

Declaration of Competing Interest

The authors declare that they have no known competing financial interests or personal relationships that could have appeared to influence the work reported in this paper.

Acknowledgments

The authors are grateful to the Science and Technology Development Plan of Jilin Province (2018020102GX), the National Key Research and Development Program of China (2017YFC0822403) and the Jilin Province and the Chinese Academy of Sciences Cooperation in Science and Technology High-tech Industrialization Special Funds Project (2018SYHZ0004).

References

- [1] Wenrui Wang, Ang Li, Qinwen Li, et al, Virtual Semi-active Damping Learning Control for Robot Manipulators Interacting with Unknown Environment, J. Vib. Control (2020), <https://doi.org/10.1016/j.ymsp.2021.107819>.
- [2] Mahmoud Ahmadinejad, Alireza Jafarisirizi, Reza Rahgozar, Effects of Shape Memory Alloys on Response of Steel Structural Buildings within Near Field Earthquakes Zone, Civil Eng. J. 6 (7) (2020) 1314–1327, <https://doi.org/10.28991/cej-2020-03091550>.

- [3] Li Zhijun et al, Asymmetric Bimanual Control of Dual-Arm Exoskeletons for Human-Cooperative Manipulations, *IEEE T ROBOT.* 34 (1) (2018) 264–271, <https://doi.org/10.1109/TRO.2017.2765334>.
- [4] M. Verma, M.V. Sivaselvan, Impedance matching control design for the benchmark problem in real-time hybrid simulation, *Mech. Syst. Signal Process* 134 (2019), <https://doi.org/10.1016/j.ymsp.2019.106343> 106343.
- [5] Alexandru Tiganescu, Bogdan Grecu, Iolanda Gabriela Craifaleanu, Dynamic Identification for Representative Building Typologies: Three Case Studies from Bucharest Area, *Civil Eng. J.* 6 (3) (2020) 418–430, <https://doi.org/10.28991/cej-2020-03091480>.
- [6] Jia Ma et al, A data-driven normal contact force model based on artificial neural network for complex contacting surfaces, *Mech. Syst. Signal Process* 156 (2021), <https://doi.org/10.1016/j.ymsp.2021.107612> 107612.
- [7] J. Ma, G. Chen, L. Ji, et al, A general methodology to establish the contact force model for complex contacting surfaces, *Mech. Syst. Signal Process* 140 (2020), <https://doi.org/10.1016/j.ymsp.2020.106678> 106678.
- [8] H. Fernando, J.A. Marshall, J. Larsson, et al, Iterative Learning-Based Admittance Control for Autonomous Excavation, *J. Intell. Robot Syst.* 96 (3) (2019) 493–500, <https://doi.org/10.1007/s10846-019-00994-3>.
- [9] Li Xiang, Y.H. Liu, H. Yu, Iterative learning impedance control for rehabilitation robots driven by series elastic actuators, *Automatica* 90 (2018) 1–7, <https://doi.org/10.1016/j.automatica.2017.12.031>.
- [10] He Wei, Yiting Dong, Adaptive fuzzy neural network control for a constrained robot using impedance learning, *IEEE T Neur Net Lear* 29 (4) (2017) 1174–1186, <https://doi.org/10.1109/TNNLS.2017.2665581>.
- [11] J. Peng, Z. Yang, T. Ma, Position/Force Tracking Impedance Control for Robotic Systems with Uncertainties Based on Adaptive Jacobian and Neural Network, *Complexity* (2019) 1–16, <https://doi.org/10.1155/2019/1406534>.
- [12] Buchli, Jonas, et al, Learning variable impedance control, *INT J ROBOT RES* 30 (7) (2011) 820–833. DOI: 10.1177/0278364911402527..
- [13] J. Luo, E. Solowjow, C. Wen, et al, Reinforcement Learning on Variable Impedance Controller for High-Precision Robotic Assembly, in: 2019 International Conference on Robotics and Automation(ICRA), IEEE, 2019, pp. 3080–3087, <https://doi.org/10.1109/ICRA.2019.8793506>.
- [14] N. Diolaiti, C. Melchiorri, S. Stramigioli, Contact impedance estimation for robotic systems, *IEEE T Robot.* 21 (5) (2005) 925–935, <https://doi.org/10.1109/TRO.2005.852261>.
- [15] Runhua Wang, Xuebo Zhang, Yongchun Fang, Visual tracking of mobile robots with both velocity and acceleration saturation constraints, *Mech. Syst. Signal Process* 150 (2021), <https://doi.org/10.1016/j.ymsp.2020.107274> 107274.
- [16] D. Verscheure, J. Swevers, H. Bruyninckx, et al, On-line identification of contact dynamics in the presence of geometric uncertainties, in: 2008 International Conference on Robotics and Automation(ICRA), IEEE, 2008, pp. 851–856, <https://doi.org/10.1109/ROBOT.2008.4543311>.
- [17] Xiaowang Chen, Zhipeng Feng, Order spectrum analysis enhanced by surrogate test and Vold-Kalman filtering for rotating machinery fault diagnosis under time-varying speed conditions, *Mech. Syst. Signal Process.* 154 (2021), <https://doi.org/10.1016/j.ymsp.2020.107585> 107585.
- [18] D. Verscheure, I. Sharf, H. Bruyninckx, et al, Identification of Contact Parameters from Stiff Multi-point Contact Robotic Operations, *Int. J. Robot RE.* 29 (4) (2010) 367–385, <https://doi.org/10.1177/0278364909336805>.
- [19] Q. Liu, J. Liang, O. Ma, A physics-based and data-driven hybrid modeling method for accurately simulating complex contact phenomenon, *Multibody Syst. Dyn* 50 (2020) 97–117, <https://doi.org/10.1007/s11044-020-09746-w>.
- [20] Menghua Zhang, Xingjian Jing, Switching logic-based saturated tracking control for active suspension systems based on disturbance observer and bioinspired X-dynamics, *Mech. Syst. Signal Process* 155 (2021), <https://doi.org/10.1016/j.ymsp.2021.107611> 107611.
- [21] Z. Doulgeri, G. Iliadis, Contact stability analysis of a one degree-of-freedom robot using hybrid system stability theory, *Robotica* 23 (5) (2005) 607–614, <https://doi.org/10.1017/S0263574704001201>.
- [22] D. Heck, A. Saccon, N. Van de Wouw, et al, Guaranteeing stable tracking of hybrid position-force trajectories for a robot manipulator interacting with a stiff environment, *Automatica* 63 (2016) 235–247, <https://doi.org/10.1016/j.automatica.2015.10.029>.
- [23] R. Kikuuwe, T. Yoshikawa, Recognizing object surface properties using impedance perception, *Robotica* 23 (2005) 387–396, <https://doi.org/10.1017/S0263574704000918>.
- [24] F. Caccavale, P. Chiacchio, A. Marino, L. Villani, Six-DOF Impedance Control of Dual-Arm Cooperative Manipulators, *IEEE-ASME T MECH.* 13 (5) (2008) 576–586, <https://doi.org/10.1109/TMECH.2008.2002816>.
- [25] Stegall Paul, D. Zanotto and S.K. Agrawal, Variable Damping Force Tunnel for Gait Training Using ALEX III, *IEEE RA-L* 2 (3) (2017) 1495–1501. DOI: 10.1109/LRA.2017.2671374..
- [26] Andrei Neculai, An adaptive scaled BFGS method for unconstrained optimization, *Numer Algor* 77 (2) (2017) 413–432, <https://doi.org/10.1007/s11075-017-0321-1>.
- [27] Abdi Fatemeh, F. Shakeri, A globally convergent BFGS method for pseudo-monotone variational inequality problems, *Optim. Method Softw.* 34 (1) (2019) 25–36. DOI: 10.1080/10556788.2017.1332619..
- [28] Ioannis E Livieris, An advanced active set L-BFGS algorithm for training weight-constrained neural networks, *Neural Comput. Appl.* 32 (2020) 6669–6684, <https://doi.org/10.1007/s00521-019-04689-6>.
- [29] Liao Aiping, Modifying the BFGS method, *Oper. Res. Lett.* 20 (4) (1997) 171–177, [https://doi.org/10.1016/S0167-6377\(96\)00050-8](https://doi.org/10.1016/S0167-6377(96)00050-8).
- [30] Richard H. Byrd, J. Nocedal, A Tool for the Analysis of Quasi-Newton Methods with Application to Unconstrained Minimization, *SIAM J. Numer. Anal.* 26 (3) (1989) 727–739, <https://doi.org/10.1137/0726042>.
- [31] C. Liu Dong, J. Nocedal, On the limited memory BFGS method for large scale optimization, *Math. Program.* 45 (1) (1989) 503–528, <https://doi.org/10.1007/BF01589116>.
- [32] Soheil Ganjefar, Sara Rezaei, Farzad Hashemzadeh, Position and force tracking in nonlinear teleoperation systems with sandwich linearity in actuators and time-varying delay, *Mech. Syst. Signal Process* 86 (2017) 308–324, <https://doi.org/10.1016/j.ymsp.2016.09.023>.
- [33] Fatemeh Rahimi, Reza Aghayari, Bijan Samali, Application of tuned mass dampers for structural vibration control: a state-of-the-art review, *Civil Eng. J.* 6 (8) (2020) 1622–1651, [10.28991/cej-2020-03091571](https://doi.org/10.28991/cej-2020-03091571).